Applied Physics Letters

Zinc gallate spinel dielectric function, band-to-band transitions, and Γ-point effective mass parameters

Cite as: Appl. Phys. Lett. **118**, 132102 (2021); https://doi.org/10.1063/5.0043686
Submitted: 11 January 2021 . Accepted: 10 March 2021 . Published Online: 30 March 2021

Matthew Hilfiker, Megan Stokey, Rafał Korlacki, Ufuk Kilic, Zbigniew Galazka, Klaus Irmscher, Stefan Zollner, and Mathias Schubert

Applied Physics Letters ARTICLE scitation.org/journal/apl

Zinc gallate spinel dielectric function, band-to-band transitions, and Γ-point effective mass parameters

Cite as: Appl. Phys. Lett. **118**, 132102 (2021); doi: 10.1063/5.0043686
Submitted: 11 January 2021 · Accepted: 10 March 2021 ·
Published Online: 30 March 2021

Matthew Hilfiker,[1,a)] Megan Stokey,[1] Rafał Korlacki,[1] Ufuk Kilic,[1] Zbigniew Galazka,[2] Klaus Irmscher,[2] Stefan Zollner,[3] and Mathias Schubert[1,4,5]

AFFILIATIONS

[1]Department of Electrical and Computer Engineering, University of Nebraska-Lincoln, Lincoln, Nebraska 68588, USA
[2]Leibniz-Institut für Kristallzüchtung, 12489 Berlin, Germany
[3]Department of Physics, New Mexico State University, Las Cruces, New Mexico 88003, USA
[4]Department of Physics, Chemistry and Biology, Linköping University, 58183 Linköping, Sweden
[5]Leibniz Institut für Polymerforschung e.V., 01069 Dresden, Germany

[a)]Author to whom correspondence should be addressed: mhilfiker2@unl.edu. URL: http://ellipsometry.unl.edu

ABSTRACT

We determine the dielectric function of the emerging ultrawide bandgap semiconductor $ZnGa_2O_4$ from the near-infrared (0.75 eV) into the vacuum ultraviolet (8.5 eV) spectral regions using spectroscopic ellipsometry on high quality single crystal substrates. We perform density functional theory calculations and discuss the band structure and the Brillouin zone Γ-point band-to-band transition energies, their transition matrix elements, and effective band mass parameters. We find an isotropic effective mass parameter ($0.24\,m_e$) at the bottom of the Γ-point conduction band, which equals the lowest valence band effective mass parameter at the top of the highly anisotropic and degenerate valence band ($0.24\,m_e$). Our calculated band structure indicates the spinel $ZnGa_2O_4$ is indirect, with the lowest direct transition at the Γ-point. We analyze the measured dielectric function using critical-point line shape functions for a three-dimensional, M_0-type van Hove singularity, and we determine the direct bandgap with an energy of 5.27(3) eV. In our model, we also consider contributions from Wannier–Mott type excitons with an effective Rydberg energy of 14.8 meV. We determine the near-infrared index of refraction from extrapolation (1.91) in very good agreement with results from recent infrared ellipsometry measurements ($\sqrt{\varepsilon_\infty} = 1.94$) [M. Stokey, Appl. Phys. Lett. **117**, 052104 (2020)].

Conductive oxides are of general interest due to their suitability for many advanced electronic and optoelectronic devices.[1–3] Of such materials, the ternary Ga-based spinel $ZnGa_2O_4$ (zinc gallate; ZGO) has recently gained attention due to the similarity of its large bandgap value to the ultrawide bandgap material β-Ga_2O_3.[4,5] The latter is currently intensely investigated because it has shown strong potential for use in high-power, high-voltage electronic applications.[5–8] ZGO may possess similar potential due to its ultrawide bandgap and its demonstrated ability to control conductivity.[4] Due to its isotropic spinel structure, ZGO may be considered preferable for device designs over the intricate anisotropic structure-property relationships in monoclinic β-Ga_2O_3.

When doped with transition metal elements, ZGO makes a promising bright, long-lasting phosphor, which is suitable for *in vivo* imaging using x-ray phosphorescence and thermally stimulated luminescence. ZGO is often investigated in nanopowders and polycrystalline materials.[9] Galazka *et al.* reported successful growth of single crystal high quality bulk ZGO and found conveniently controllable electrical conductivity.[4] Melt-grown crystals can be either electrically insulating or highly conducting with the free electron concentration approaching $10^{20}\,cm^{-3}$ and Hall electron mobility of about $100\,cm^2/V\,s$ at such high free electron concentrations.[4] Although the optical and electrical properties of ZGO play a fundamental role in its potential use for the aforementioned applications, such inherent properties were seldomly discussed in the literature. Infrared and Raman active phonon mode properties have been explored both computationally and experimentally.[10–15] Stokey *et al.* reported the first complete set of infrared and Raman active mode parameters for ZGO using a combined

spectroscopic ellipsometry and density functional theory (DFT) computational analysis.[16] Electronic band structure properties, band-to-band transitions, and crystal structure[17] have been computationally studied previously (see, e.g., Zeraga *et al.*[18] and Galazka *et al.*[4]). A broad range of calculated fundamental bandgap energies can be found in the literature, and agreement seems to have been reached on the indirect bandgap nature of ZGO.[19–21] Brik reported the lowest indirect Γ–L transition at 4 eV and the lowest direct Γ-point transition at 4.2 eV.[22] Attempts were made to calculate the spectral dependence of the dielectric function and complex index of refraction.[18,21,22] Early diffuse reflectance spectroscopy and transmittance studies of polycrystalline ZGO reported an approximate bandgap energy of 4.6…5 eV.[23–25] Galazka *et al.* reported transmittance and reflectance investigations on single crystal ZGO and determined the bandgap energy at 4.6 eV. The authors also estimated an index of refraction of 1.90 and 1.97 at 2 and 1 μm wavelengths, respectively.[4] This value compares well with the square root of the high-frequency dielectric constant, $\sqrt{\varepsilon_\infty} = 1.94$, determined by Stokey *et al.* using infrared ellipsometry.[16] No characterization of the complex valued dielectric function of ZGO in the near-infrared to deep ultraviolet spectral region has been reported. It is well known that band-to-band transitions and associated exciton contributions cause critical point (CP) structures within the dielectric function, and model line shape analysis can determine accurately band-to-band transition and exciton properties.[26] In this work, we report the dielectric function of ZGO and we perform a CP analysis in combination with DFT calculations.

Plane-wave code Quantum ESPRESSO[27] was used to perform DFT calculations using a combination of norm-conserving Troullier–Martins pseudopotentials, generated using FHI98PP,[28,29] available from the Quantum ESPRESSO pseudopotentials library, and generalized-gradient-approximation (GGA) density functional of Perdew *et al.*[30] The semicore 3*d* states of gallium were not included in the valence configuration. All calculations were performed using a high electronic wavefunction cutoff of 300 Ry. The equilibrium geometry was obtained as in our previous work.[16] The initial structure was first relaxed to force levels less than 10^{-6} Ry Bohr^{-1}. A shifted $4 \times 4 \times 4$ Monkhorst-Pack[31] grid was used for sampling of the Brillouin zone and a convergence threshold of 1×10^{-12} Ry was used to reach self-consistency. Additional calculations were then performed at the equilibrium geometry. To study the band structure, we used the band interpolation method based on the maximally localized Wannier functions[32,33] as implemented in the software package WANNIER90.[34] The entire Brillouin zone was sampled using a non-shifted $8 \times 8 \times 8$ grid with a convergence threshold of 1×10^{-10} Ry. The initial projectors for the Wannier functions were automatically generated using the selected columns of the density matrix (SCDM)[35] method treating the valence band as isolated. The plot of the band structure of the valence band is shown in Fig. 1, while the color-coded contributions of atomic wavefunctions to energy bands, prepared using PyProcar,[36] for both the valence and the conduction bands are shown in Fig. 2. The interpolated band structure was used to obtain the effective mass parameters for selected bands. Each band was plotted in high resolution in the range ± 0.01 Å^{-1} around the Brillouin zone center and the band energy vs reciprocal distance was fitted using a second order polynomial. The values of the effective mass were extracted from the quadratic term coefficients according to the equation

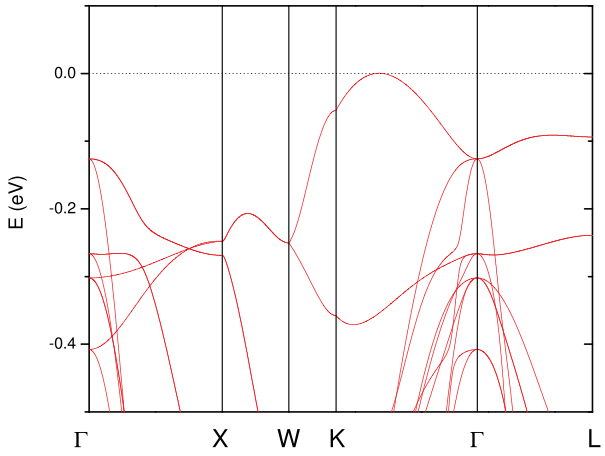

FIG. 1. DFT/GGA structure of the valence band of $ZnGa_2O_4$ (ZGO) in the vicinity of the Γ-point. The position of the bands on the energy scale was adjusted so that the valence band maximum appears at $E = 0$. Definition of high-symmetry points as in Ref. 44 (FCC lattice).

$$(m^{\star-1})_{jj} = \frac{1}{\hbar^2}\frac{\partial^2}{\partial k_j^2}E(\mathbf{k}), \tag{1}$$

where derivatives are taken along the high symmetry directions in the reciprocal space, i.e., Γ–L, Γ–K, and Γ–X. The values of the obtained effective mass parameters are listed in Table I. Because the top three valence bands are degenerate at Γ, states within the band of the highest curvature are assumed to couple with Γ-point conduction band states during exciton formation under optical band-to-band transition excitation. The curvature is the strongest along all equivalent Γ–L directions, with an effective hole mass parameter of 0.24 m_e. This value is used for the calculation of the exciton binding energy.

Single crystal ZGO was grown using the vertical gradient freeze (VGF) method, and the details are provided by Galazka *et al.*[4] The fabricated wafer for the present study was electrically insulating, double-side polished with a principal (111) surface and dimensions of 10 mm × 10 mm × 0.5 mm. Spectroscopic ellipsometry determines the change in polarization state of light upon interaction with a sample. Ellipsometry measures two values (Ψ, Δ), which correspond to the amplitude ratio and phase difference, respectively, of the ratio of the complex valued *p* and *s* polarized Fresnel reflection coefficients, $\tan\Psi \exp(i\Delta) = r_p/r_s$.[37] A dual-rotating compensator ellipsometer (RC2, J. A. Woollam Co., Inc.) was used to acquire data in the spectral range of 0.73 eV–6.42 eV. Measurements were performed at ambient temperature for four angles of incidence ($\Phi_a = 45°$, 55°, 65°, and 75°). To measure data in the vacuum-ultra-violet (VUV) spectral region, a rotating-analyzer ellipsometer with an automated compensator function (VUV-VASE, J.A. Woollam Co., Inc.) was used. The VUV-VASE measured data for the spectral range of 5 eV–8.5 eV were measured in steps of 0.01 eV at four angles of incidence ($\Phi_a = 45°$, 55°, 65°, and 75°).

A substrate-overlayer model approach is used to describe the substrate along with the effects of a nanoscale surface roughness. The effects of the surface roughness onto the ellipsometric parameters are modeled by using optical constants for the overlayer obtained as the average of the substrate optical constants and the ambient.[37] Then,

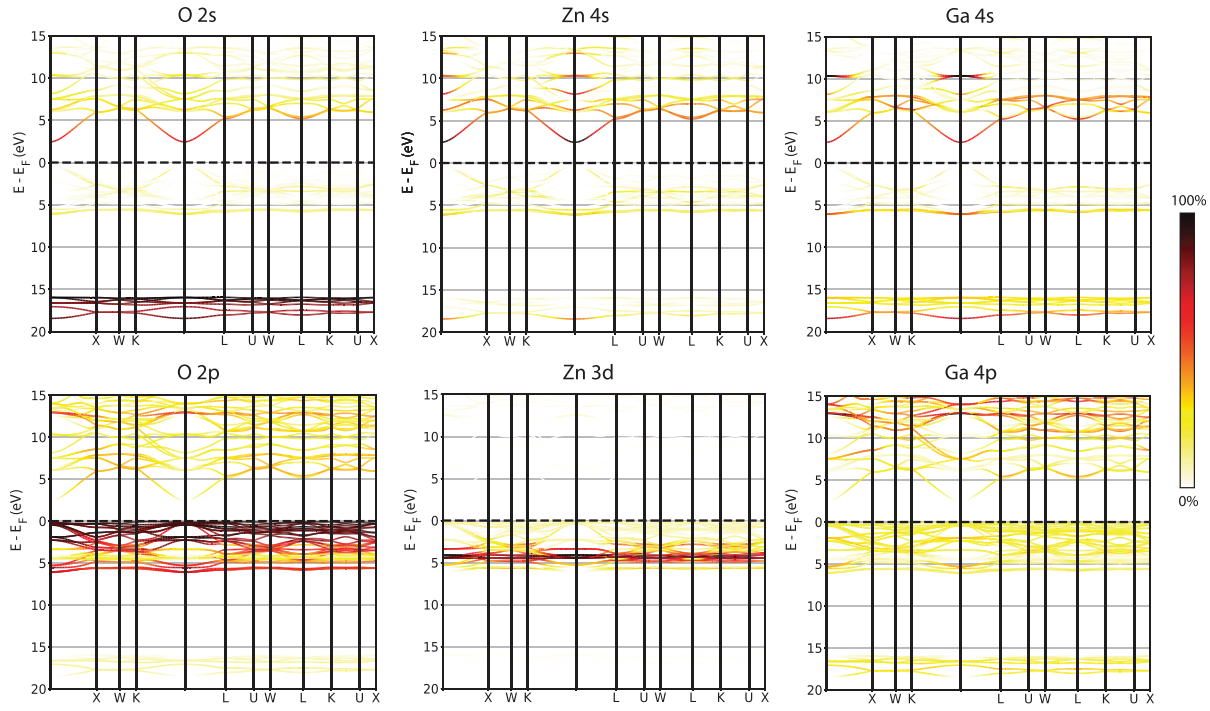

FIG. 2. Color-plot density distributions of oxygen 2*s* and 2*p*, zinc 4*s* and 3*d*, and gallium 4*s* and 4*p* level contributions to DFT/GGA calculated valence and conduction bands in ZGO along a high-symmetry path through the Brillouin zone. Definitions of high-symmetry points as in Ref. 44 (FCC lattice). Similar to Fig. 1, the energy scale was shifted so that the valence band maximum appears at $E = 0$.

initially, a Cauchy dispersion equation is applied to model the optical constants of the ZGO substrate in the transparent region ($\leq$ 3 eV) where absorption is extremely small and can be assumed to not affect the ellipsometric parameters. This allows for the surface roughness overlayer thickness parameter, t_{ov}, to be determined. This parameter is then fixed, and a point-by-point (PBP) regression analysis for the determination of the wavelength-by-wavelength dielectric function of ZGO is performed. The PBP determined dielectric function is analyzed using a CP model dielectric function (MDF) approach. Each CP model contribution accounts for certain band-to-band transitions and their associated van-Hove singularities within the joint density of states.[26,37] We observe three major contributions for ZGO in the spectral range investigated here, (i) a direct band-to-band transition associated with a M_0-type van Hove singularity, (ii) an exciton associated with a M_0-type transition, and (iii) a combined contribution from high-energy band-to-band transitions with non-identifiable van Hove singularities. The fundamental bandgap transition found in ε is modeled using a M_0-type CP structure[26,38,39]

$$\varepsilon_{(M_0)} = AE^{-1.5}\chi^{-2}\left[2 - (1+\chi)^{0.5} - (1-\chi)^{0.5}\right], \tag{2}$$

$$\chi = \frac{\hbar\omega + i\Gamma}{E}, \tag{3}$$

where $\hbar\omega$ is the photon energy and A, E, and Γ denote the CP amplitude, transition energy, and broadening parameter, respectively. Contributions from Wannier–Mott type excitons to the lowest CP structure are described here with an anharmonically broadened Lorentz oscillator[26,40,41]

$$\varepsilon_{(ex)} = \frac{A^2 - ib\hbar\omega}{(E - R^\star)^2 - (\hbar\omega)^2 - i\Gamma\hbar\omega}, \tag{4}$$

where b denotes the anharmonic broadening parameter, and $R^\star$ is the effective Rydberg energy,

$$R^\star = 13.6\,eV\frac{\mu}{m_e\varepsilon_{DC}^2}, \tag{5}$$

TABLE I. DFT/GGA Γ-point band effective mass parameters obtained in this work according to Eq. (1) in units of free electron mass, m_e, for the directions $\Gamma - L$, $\Gamma - K$, and $\Gamma - X$. Values for the lowest conduction band ($c = 1$) are also compared with Sampath *et al.* (tight-binding linearized muffin-tin orbital method).[19] The Γ-point effective electron mass parameters render an isotropic tensor in Eq. (1). The top three valence bands are highly anisotropic and degenerate at Γ, where states within the band of strongest curvature are assumed to couple with conduction band states during exciton formation, with an effective hole mass parameter of 0.24 m_e accordingly.

Band index	$m_{\Gamma-L}/m_e$	$m_{\Gamma-K}/m_e$	$m_{\Gamma-X}/m_e$
$c = 1$	0.24	0.24	0.24
$c = 1$	0.21[a]	0.23[a]	0.22[a]
$v = 1$	3.68	2.00	−5.48
$v = 2$	3.68	−5.42	−5.42
$v = 3$	−0.24	−0.26	−0.31

[a]Reference 19.

and μ is the reduced effective conduction and valence band mass, m_e is the free electron mass, and ε_{DC} is the static dielectric permittivity.[26] Using our previously determined value for $\varepsilon_{DC} = 10.5$[16] and our DFT calculated Γ-point effective hole ($0.24\,m_e$) and electron ($0.24\,m_e$) mass parameters (See Table I), we estimate $R^\star = 14.8$ meV. This value is used for our ellipsometry data analysis and not further varied. It is comparable to the exciton binding energy parameters at the fundamental gap energy of conventional semiconductors, such as GaAs (4.4 meV) and GaN (32 meV),[26] but is much smaller than exciton energies of the recently characterized,[41] monoclinic symmetry ultra-wide bandgap semiconductor β-Ga_2O_3 (120 meV, 229 meV, and 178 meV).[42] For rhombohedral structure Ga_2O_3, we recently obtained a similar small exciton energy for the fundamental band-to-band transition (7 meV) while the second band-to-band transition that causes a two dimensional critical point is associated with a hyperbolic exciton of 178 meV.[43] Note that we only consider the first excitonic contribution, $R_n = R^\star/n^2$, for $n = 1$ because higher order contributions for $n > 1$ rapidly decay in amplitude. Higher energy CP contributions to the ZGO dielectric function are modeled with a Gaussian broadened oscillator. Such broadened features often contain contributions from multiple, neighboring energy transitions within the Brillouin zone. We use a Gaussian broadened oscillator here to define the imaginary ($\Im$) part[37,39]

$$\Im\{\varepsilon_{(G)}\} = A\left(e^{-\left[\frac{\hbar\omega-E}{\sigma}\right]^2} - e^{-\left[\frac{\hbar\omega+E}{\sigma}\right]^2}\right), \tag{6}$$

$$\sigma = \Gamma/(2\sqrt{ln(2)}), \tag{7}$$

where from Kramers–Kronig integration the real part is obtained

$$\Re\{\varepsilon_{(G)}\} = \frac{2}{\pi} P \int_0^\infty \frac{\xi \Im\{\varepsilon_{(G)}\}}{\xi^2 - (\hbar\omega)^2} d\xi. \tag{8}$$

The allowed optical transitions at the Brillouin zone center were identified in DFT calculations by extracting matrix elements of the momentum operator between the valence and conduction bands, $|\mathscr{M}_{cv}|^2$. We restrict our analysis to the transitions at the Brillouin zone center because the transitions at other high symmetry points occur at much larger energies than investigated here. For more accurate transition energies, this calculation was performed using the hybrid Gau-PBE[45,46] density functional, at the PBE equilibrium geometry described above, using a regular non-shifted $8 \times 8 \times 8$ Monkhorst-Pack grid for Brillouin zone sampling and a coarser $4 \times 4 \times 4$ grid for sampling of the Fock operator. The convergence threshold for self-consistency was 1×10^{-10} Ry. Table II summarizes DFT calculated Γ-point direct (vertical) band-to-band transition energies, Γ_{c-v}, and transition matrix elements, $|\mathscr{M}_{cv}|^2$, for all identified transitions in the energy range up to 10 eV. For multiple transitions occurring at the same photon energy due to degenerate bands, the value of the matrix element is the sum of all the contributing transitions. The two lowest transitions involve the lowest conduction band and are predicted at 4.816 eV and 7.142 eV. The second transition, however, has a much smaller transition matrix element. A group of transitions above 8 eV is dominated by one strong transition matrix element at 8.801 eV, accompanied by transitions with much smaller matrix elements. Figure 1 depicts the valence band structure of ZGO. As can be seen from the top most valence band structure, ZGO is indirect with the valence band maximum near the K-point and conduction band minimum at Γ. Near the Γ-point, the top most valence bands turn upward toward K and L points. However, due to the small conduction band effective mass parameters in the same directions, the combined conduction and valence bands' $E_{CB}(\mathbf{k}) - E_{VB}(\mathbf{k})$ curvatures (reduced or optical mass parameters) at Γ are all positive, giving rise to the M_0-type singularity in the combined density of states. We note that indirect transitions only weakly contribute to the dielectric function and, hence, we cannot determine their properties from our dielectric function measurements.

TABLE II. Hybrid-level-DFT Γ-point direct band-to-band transition energies, Γ_{c-v}, and transition matrix elements, $|\mathscr{M}_{cv}|^2$. Indices are labeled from the bandgap, i.e., for conduction bands increasing with energy starting with $c = 1$ for the lowest conduction band and for valence bands decreasing in energy starting with $v = 1$ for the highest band.

Label	E (eV)	$\lvert\mathscr{M}_{cv}\rvert^2$ $(\hbar/\text{Bohr})^2$	c	v
$\Gamma_{1-1}+\Gamma_{1-2}+\Gamma_{1-3}$	4.816	0.47 192 256	1	1,2,3
$\Gamma_{1-15}+\Gamma_{1-16}+\Gamma_{1-17}$	7.142	0.04 084 615	1	15,16,17
$\Gamma_{2-1}+\Gamma_{2-2}+\Gamma_{2-3}+\Gamma_{3-1}+\Gamma_{3-2}+\Gamma_{3-3}+\Gamma_{4-1}+\Gamma_{4-2}+\Gamma_{4-3}$	8.239	0.07 402 964	2,3,4	1,2,3
$\Gamma_{5-4}+\Gamma_{5-5}+\Gamma_{5-6}$	8.801	0.50 129 614	5	4,5,6
$\Gamma_{1-25}+\Gamma_{1-26}+\Gamma_{1-27}$	9.856	0.07 359 619	1	25,26,27

Figure 2 depicts distributions of the O 2s, 2p, Zn 4s, 3d, and Ga 4s, 4p levels contributing to valence and conduction bands. The top of the valence band is predominantly formed by oxygen 2p levels, while the bottom of the conduction band mostly consists of s contributions from all elements. This explains the mostly isotropic shape in the vicinity of the parabolic minimum at the Γ-point. Furthermore, we note that lower lying bands at the top of the valence bands are also predominantly formed by oxygen 2p levels and p-orbital interaction may explain the strong warping of the valence bands ultimately leading to the indirect gap in ZGO. We also note that the DFT/GGA band structure underestimates the energy gap between the valence and the conduction band. Therefore, as described above, Γ-point direct band-to-band transition energies, Γ_{c-v}, and transition matrix elements, $|\mathscr{M}_{cv}|^2$, which are shown in Table II, are determined at a higher level of theory using a hybrid density functional. The effective mass parameters for all valence and conduction bands contributing to the lowest transitions are noted in Table I.

Figure 3 depicts experimental and best-match model calculated ellipsometry data (Ψ, Δ), in excellent agreement with each other. As a result of this step, we determined the overlayer roughness $t_{ov} = 2.3$ nm. A distinct feature at about 5 eV emerges from the spectra, which points to the onset of strong absorption due to a band-to-band transition. Figure 4 shows the PBP determined dielectric function (green dashed lines) together with the best-model calculated MDF approach. A sum of CP contributions is used for ZGO here, $\varepsilon = \varepsilon_{off} + \varepsilon_{(M_0)} + \varepsilon_{(ex)} + \varepsilon_{(G)}$, where we added a small constant offset value, ε_{off}. An excellent, virtually identical match between the two datasets is seen. Also shown in Fig. 4 are the individual contributions for the imaginary parts from each MDF component. We note that the exciton model contribution imaginary part is negative over a limited spectral region as a result of anharmonic coupling. Two resonant processes when coupled anharmonically produce a phase shift between their oscillatory behaviors

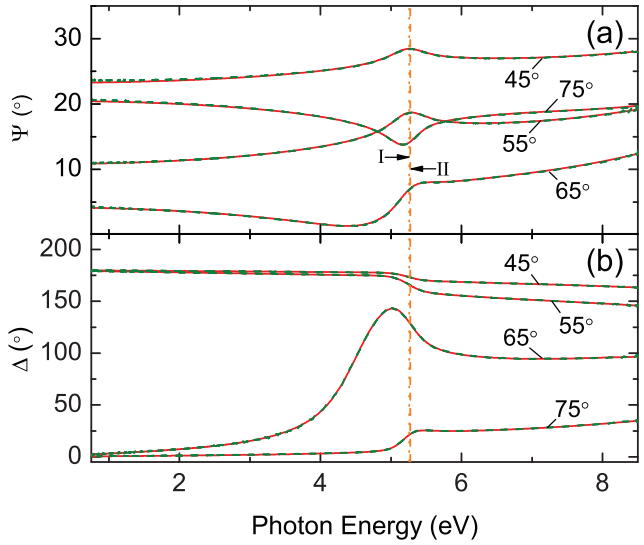

FIG. 3. (a) Psi and (b) delta data measured by experiment (green dashed lines) and obtained from best-match model calculations (red solid lines). Labels indicate the angles of incidence. The vertical dotted and dashed lines with roman symbols I and II indicate the spectral center energy position for $CP^{(0x)}$ and $CP^{(0)}$, $E - R^{\star}$, and E, respectively. Note that both vertical lines are virtually indistinguishable since $R^{\star} = 14.8$ meV $\ll E = 5.273$ eV.

due to exchange of excitation energy. As a result, individual contributions may appear to show gain, while the sum of both processes obeys passivity principles,[47] i.e., positive imaginary parts throughout. A similar observation was reported previously for the alpha-phase of gallium oxide.[43] A vertical line indicates the fundamental band-to-band transition energy. All best-match model parameters are listed in Table III. We identify the energy of the higher-energy CP structure just about

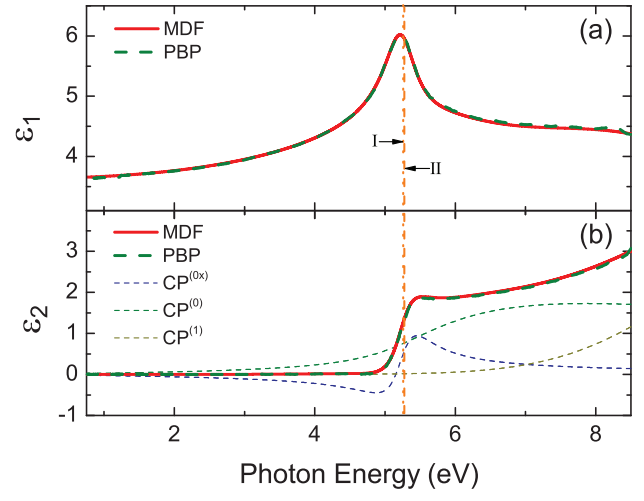

FIG. 4. (a) Real and (b) imaginary components of the dielectric function determined by point-by-point (PBP; green dashed lines) and best-match calculated model (MDF; red lines) for zinc gallate obtained in this work. See Fig. 3 for meaning and labels of vertical dotted and dashed lines.

TABLE III. Best-match CP model parameters from MDF analysis, amplitude (A), energy (E), and harmonic (Γ) and anharmonic (b) broadening parameters. $\varepsilon_{off} = 1.080(3)$. The last digit is determined with 90% confidence, which is indicated with parentheses for each parameter. A weighted least mean square approach is used as described by Fujiwara.[37] Small confidence intervals are indicative for the excellent match between model and experiment obtained here. Note that parameters E are identical for $CP^{(0x)}$ and $CP^{(0)}$. We used our calculated exciton binding energy $R^{\star} = 14.8$ meV, which was not varied during MDF analysis.

Critical point analysis				
	A	E (eV)	Γ (eV)	b (eV)
$CP^{(0x)}$	1.20(1) (eV^2)	5.27(3)[a]	0.556(1)	0.736(2)
$CP^{(0)}$	79.31(7) ($eV^{1.5}$)	5.27(3)	0.746(4)	…
$CP^{(1)}$	3.36(1)	11.09(1)	4.19(1)	…

outside our spectral range, and our analysis finds its CP center energy by extrapolation at 11.09(1) eV. The effective Rydberg energy for the M_0-type transition is used here with $R^{\star} = 14.8$ meV according to our DFT calculations discussed above. The direct bandgap energy $E_0 = 5.27(3)$ eV compares well with our lowest hybrid-level-DFT calculated transition at 4.816 eV. The next higher calculated transition at 7.142 eV has small transition matrix element and may be subsumed by the fundamental gap CP feature. The group of transitions predicted at 8.239 eV, 8.801 eV, and 9.856 eV may be responsible for the higher-energy CP structure identified here with a Gaussian contribution and centered at approximately 11.09(1) eV. Galazka *et al.* reported below-bandgap absorption coefficient spectra plotted in power two vs photon energy and which indicated a direct transition gap energy of 4.59 ± 0.03 eV. Absorption measurements performed on this sample in the present work revealed a similar onset of absorption indicative for an absorption process onset at about 4.6 eV. However, the absorption is very small and can only be followed experimentally over a limited spectral range because of the large sample thickness (250 μm in Ref. 4 and 500 μm in this work). The indirect transition estimated from our band structure calculations originating from the valence band maximum along the K–Γ direction is approximately 130 meV smaller than the direct transition. Thus, the observed absorption onset approximately 700 meV below the direct transition at 5.273 eV cannot likely be due to the indirect transition. We hypothesize that a defect-related process may cause the onset of absorption detected in transmission across the thick samples and for which we do not presently know the physical origin. We emphasize that in order to investigate the absorption coefficient within the bandgap, for which ellipsometry has limited sensitivity because it is too small, the spectral transmittance loss of a series of samples with decreasing thickness will need to be investigated in search for signatures due to the indirect band-to-band transition. ZGO reveals a relatively low dispersive index of refraction ($n = \sqrt{\varepsilon}$) over a long spectral range of transparency from the phonon mode range (not shown here) until its onset of the excitonic absorption. If we use our MDF and extrapolate the index of refraction for $\hbar\omega \to 0$, we obtain $n = 1.91$, which is in very good agreement with the high-frequency extrapolation from infrared ellipsometry measurements ($n = 1.94$)[16] and transmittance measurements at wavelengths of 1 μm (1.97) and 2 μm (1.90).[4] In addition, we note that very little resemblance exists between computationally obtained optical functions spectra for ZGO previously reported and our results.[18,21,22]

In summary, we have determined the dielectric function of ZGO from the near-infrared to the vacuum ultraviolet. We identify the lowest direct band-to-band transition and its associated exciton contribution using a critical point model approach. We also identify a group of higher energy transitions, and we compare our results with band structure, density of states, and transition energies obtained from a DFT computational study. ZGO is an ultrawide bandgap semiconductor, with a three-dimensional singularity at the Γ-point bandgap and an exciton contribution with Wanier–Mott type exciton energy. We also provided an accurate index of refraction and extinction coefficient values over the entire spectrum of interest.

This work was supported in part by the National Science Foundation under award DMR 1808715, in the framework of GraFOx, a Leibniz-Science Campus partially funded by the Leibniz Association-Germany, by Air Force Office of Scientific Research under Award Nos. FA9550-18-1-0360 and FA9550-19-S-0003, by the Nebraska Materials Research Science and Engineering Center under Award No. DMR 1420645, by the Swedish Knut and Alice Wallenbergs Foundation supported grant "Wide-bandgap semiconductors for next generation quantum components," and by the American Chemical Society/Petrol Research Fund. Mathias Schubert acknowledges the University of Nebraska Foundation and the J. A. Woollam Foundation for financial support. DFT calculations were in part performed at the Holland Computing Center of the University of Nebraska, which receives support from the Nebraska Research Initiative.

DATA AVAILABILITY

The data that support the findings of this study are available from the corresponding author upon reasonable request.

REFERENCES

[1]M. Grundmann, H. Frenzel, A. Lajn, M. Lorenz, F. Schein, and H. von Wenckstern, Phys. Status Solidi A **207**, 1437 (2010).
[2]M. Lorenz, M. S. R. Rao, T. Venkatesan, E. Fortunato, P. Barquinha, R. Branquinho, D. Salgueiro, R. Martins, E. Carlos, A. Liu, F. K. Shan, M. Grundmann, H. Boschker, J. Mukherjee, M. Priyadarshini, N. DasGupta, D. J. Rogers, F. H. Teherani, E. V. Sandana, P. Bove, K. Rietwyk, A. Zaban, A. Veziridis, A. Weidenkaff, M. Muralidhar, M. Murakami, S. Abel, J. Fompeyrine, J. Zuniga-Perez, R. Ramesh, N. A. Spaldin, S. Ostanin, V. Borisov, I. Mertig, V. Lazenka, G. Srinivasan, W. Prellier, M. Uchida, M. Kawasaki, R. Pentcheva, P. Gegenwart, F. M. Granozio, J. Fontcuberta, and N. Pryds, J. Phys. D: Appl. Phys. **49**, 433001 (2016).
[3]S. J. Pearton, J. Yang, P. H. Cary, F. Ren, J. Kim, M. J. Tadjer, and M. A. Mastro, Appl. Phys. Rev. **5**, 011301 (2018).
[4]Z. Galazka, S. Ganschow, R. Schewski, K. Irmscher, D. Klimm, A. Kwasniewski, M. Pietsch, A. Fiedler, I. Schulze-Jonack, M. Albrecht, T. Schröder, and M. Bickermann, APL Mater. **7**, 022512 (2019).
[5]M. Higashiwaki and G. H. Jessen, Appl. Phys. Lett. **112**, 060401 (2018).
[6]M. Higashiwaki, K. Sasaki, A. Kuramata, T. Masui, and S. Yamakoshi, Phys. Status Solidi A **211**, 2126 (2014).
[7]Z. Xia, H. Chandrasekar, W. Moore, C. Wang, A. J. Lee, J. McGlone, N. K. Kalarickal, A. Arehart, S. Ringel, F. Yang, and S. Rajan, Appl. Phys. Lett. **115**, 252104 (2019).
[8]J. Zhang, J. Shi, D.-C. Qi, L. Chen, and K. H. L. Zhang, APL Mater. **8**, 020906 (2020).
[9]X. Sun, J. Shi, X. Fu, Y. Yang, and H. Zhang, Sci. Rep. **8**, 10595 (2018).
[10]G. G. Van Gorkom, J. C. Henning, and R. P. Van Stapele, Phys. Rev. B **8**, 955 (1973).
[11]J. E. Drake and J. Simpson, Spectrochim. Acta, Part A **24**, 981 (1968).
[12]H. A. Lauwers and M. A. Herman, J. Phys. Chem. Solids **41**, 223 (1980).
[13]S. López, A. H. Romero, P. Rodríguez-Hernández, and A. Muñoz, Phys. Rev. B **79**, 214103 (2009).
[14]J. Preudhomme and P. Tarte, Spectrochim. Acta, Part A **27**, 1817 (1971).
[15]S. López-Moreno, P. Rodríguez-Hernández, A. Muñoz, A. H. Romero, F. J. Manjón, D. Errandonea, E. Rusu, and V. V. Ursaki, Ann. Phys. **523**, 157 (2011).
[16]M. Stokey, R. Korlacki, S. Knight, M. Hilfiker, Z. Galazka, K. Irmscher, V. Darakchieva, and M. Schubert, Appl. Phys. Lett. **117**, 052104 (2020).
[17]A. Bouhemadou and R. Khenata, Phys. Lett. A **360**, 339 (2006).
[18]F. Zerarga, A. Bouhemadou, R. Khenata, and S. Bin-Omran, Solid State Sci. **13**, 1638 (2011).
[19]S. K. Sampath, D. G. Kanhere, and R. Pandey, J. Phys.: Condens. Matter **11**, 3635 (1999).
[20]H. Dixit, N. Tandon, S. Cottenier, R. Saniz, D. Lamoen, B. Partoens, V. Van Speybroeck, and M. Waroquier, New J. Phys. **13**, 063002 (2011).
[21]C. Xiang, H. Tan, J. Lu, Y. Yang, and C. Ni, J. Alloys Compd. **581**, 139 (2013).
[22]M. Brik, J. Phys. Chem. Solids **71**, 1435 (2010).
[23]T. Omata, N. Ueda, K. Ueda, and H. Kawazoe, Appl. Phys. Lett. **64**, 1077 (1994).
[24]X. Chen, H. Xue, Z. Li, L. Wu, X. Wang, and X. Fu, J. Phys. Chem. C **112**, 20393 (2008).
[25]M. M. Can, G. Hassnain Jaffari, S. Aksoy, S. I. Shah, and T. Fırat, J. Alloys Compd. **549**, 303 (2013).
[26]P. Yu and M. Cardona, *Fundamentals of Semiconductors* (Springer, Berlin, 1999).
[27]P. Giannozzi, S. Baroni, N. Bonini, M. Calandra, R. Car, C. Cavazzoni, D. Ceresoli, G. L. Chiarotti, M. Cococcioni, I. Dabo, A. D. Corso, S. de Gironcoli, S. Fabris, G. Fratesi, R. Gebauer, U. Gerstmann, C. Gougoussis, A. Kokalj, M. Lazzeri, L. Martin-Samos, N. Marzari, F. Mauri, R. Mazzarello, S. Paolini, A. Pasquarello, L. Paulatto, C. Sbraccia, S. Scandolo, G. Sclauzero, A. P. Seitsonen, A. Smogunov, P. Umari, and R. M. Wentzcovitch, J. Phys.: Condens. Matter **21**, 395502 (2009).
[28]M. Fuchs and M. Scheffler, Comput. Phys. Commun. **119**, 67 (1999).
[29]N. Troullier and J. L. Martins, Phys. Rev. B **43**, 1993 (1991).
[30]J. P. Perdew, K. Burke, and M. Ernzerhof, Phys. Rev. Lett. **77**, 3865 (1996).
[31]H. J. Monkhorst and J. D. Pack, Phys. Rev. B **13**, 5188 (1976).
[32]N. Marzari and D. Vanderbilt, Phys. Rev. B **56**, 12847 (1997).
[33]I. Souza, N. Marzari, and D. Vanderbilt, Phys. Rev. B **65**, 035109 (2001).
[34]A. A. Mostofi, J. R. Yates, Y.-S. Lee, I. Souza, D. Vanderbilt, and N. Marzari, Comput. Phys. Commun. **178**, 685 (2008).
[35]V. Vitale, G. Pizzi, A. Marrazzo, J. R. Yates, N. Marzari, and A. A. Mostofi, Comput. Mater. **6**, 66 (2020).
[36]U. Herath, P. Tavadze, X. He, E. Bousquet, S. Singh, F. Muñoz, and A. H. Romero, Comput. Phys. Commun. **251**, 107080 (2020).
[37]H. Fujiwara, *Spectroscopic Ellipsometry* (John Wiley & Sons, New York, 2007).
[38]M. Schubert, T. Hofmann, B. Rheinländer, I. Pietzonka, T. Sass, V. Gottschalch, and J. A. Woollam, Phys. Rev. B **60**, 16618 (1999).
[39]*Guide to Using WVASE® Spectroscopic Ellipsometry Data Acquisition and Analysis Software* (J. A. Woollam Co., Inc., Lincoln, Nebraska, 2012).
[40]A. Mock, R. Korlacki, S. Knight, and M. Schubert, Phys. Rev. B **95**, 165202 (2017).
[41]A. Mock, R. Korlacki, C. Briley, V. Darakchieva, B. Monemar, Y. Kumagai, K. Goto, M. Higashiwaki, and M. Schubert, Phys. Rev. B **96**, 245205 (2017).
[42]The exciton energies belong to the 3 direct band-to-band transitions at the Γ-point which are polarized along axis **a** (CP_1^{ac}-CP_{1x}^{ac}=229 meV), axis **c** (CP_0^{ac}-CP_{0x}^{ac}=120 meV), and axis **b** (CP_0^{b}-CP_{0x}^{b}=178 meV). See Ref. 41.
[43]M. Hilfiker, R. Korlacki, R. Jinno, Y. Cho, H. G. Xing, D. Jena, U. Kilic, M. Stokey, and M. Schubert, Appl. Phys. Lett. **118**, 062103 (2021).
[44]W. Setyawan and S. Curtarolo, Comput. Mater. Sci. **49**, 299 (2010).
[45]J.-W. Song, K. Yamashita, and K. Hirao, J. Chem. Phys. **135**, 071103 (2011).
[46]J.-W. Song, G. Giorgi, K. Yamashita, and K. Hirao, J. Chem. Phys. **138**, 241101 (2013).
[47]D. W. Berreman and F. C. Unterwald, Phys. Rev. **174**, 791 (1968).